Investigations on performance of valveless piezoelectric micropump with concave tuning diffuser/nozzle elements in transient flow

Xiuhua He[1] ✉, *Jiawei Shi*[1], *Hang Yang*[1], *Nan Lin*[1], *Benjamin Bernard Uzoejinwa*[2]

[1]*School of Energy and Power Engineering, Jiangsu University, Zhenjiang, People's Republic of China*
[2]*Department of Agricultural and Bioresources Engineering, University of Nigeria, Nsukka, Nigeria*
✉ *E-mail: xiuhua.he@ujs.edu.cn*

Published in Micro & Nano Letters; Received on 18th November 2018; Revised on 28th January 2019; Accepted on 28th February 2019

A diffuser/nozzle is one of the most frequently-used channels in a valveless piezoelectric micropump, but its efficiency has not been satisfactory. Hence, optimisation of the channel structure is of great significance. The concave tuning diffuser/nozzle element can obtain steady flow rectification under different Reynolds numbers, and its efficiency is much higher than the conventional diffuser/nozzle element whose diverging angle is >25°. Therefore, the application of concave tuning on the micropump is promising and worth anticipating. In this work, the experiment and numerical simulation were carried out under the conditions of voltage (50–250 vpp), excitation frequency (10–1000 Hz) and Re_c (100–1000). The results show that the performance of a micropump with concave tuning is better than that with a straight sidewall, as the pump efficiency is improved significantly. The position and size of vortexes are of great significance to the pump efficiency of the micropumps. The distribution of pressure in the micropumps with concave tuning and straight sidewall was displayed. With the increase of characteristic Reynolds number, the adverse pressure gradient occurred. Compared with the straight sidewall, the concave tuning structure can better withstand adverse pressure gradient and delay the boundary layer separation in the channel.

1. Introduction: The valveless piezoelectric micropump is a kind of vibrating diaphragm pump, which conveys the working fluids based on the converse piezoelectric effect of piezoelectric material [1]. It has many proven advantages, such as small size, low power consumption and insensitivity of fluid viscosity etc. [2–4].

The efficiency of the micropump is directly determined by the flow characteristic of the microchannel [5]. A conventional diffuser/nozzle element is applied frequently in the micropump. Recently, it has been verified that the geometrical tuning of diffuser/nozzle elements is beneficial to improve the efficiency of the diffuser in steady flow. Especially, the concave tuning can obtain a steady flow rectification under different Reynolds numbers [6, 7]. However, some differences in flow characteristics exist between transient and steady flow, the results obtained from steady flow cannot be suitable for transient flow. For example, Anders Olsson *et al.* [8] reported that the flow separation in the diverging direction led to the low diffuser efficiency in steady flow. However, in transient flow, Sun *et al.* [9] and He *et al.* [10] concluded that the vortexes could contribute to the increase of pump efficiency, so the position and intensity of the vortexes play a significant role in transient flow.

In this study, the net flow and pump efficiency of a valveless piezoelectric micropump with concave tuning (concave tuning parameter: $\beta_{cv} = 2$) and a conventional diffuser/nozzle element that have the diverging angle of 30° have been investigated consecutively under the conditions of voltage (50–250 vpp) and excitation frequency (10–1000 Hz). In order to ensure a reliable simulation, the dynamic mesh method [11] was used for the simulation of the piezoelectric actuator under the conditions of different vibrator displacements and excitation frequencies. The internal flow field and pressure distribution were also revealed via the 3D finite volume method.

2. Theory and calculation

2.1. Net flow: The operating principle of the valveless piezoelectric micropump contains two stages in a period: suction process and pump process.

In the suction process, the piezoelectric vibrator moves upward and the volume of the pump chamber increases, so the fluids are sucked into the chamber from the inlet and outlet at the same time. However, the resistance coefficient of the diverging direction is smaller than that of the converging direction, so fluids sucked into the chamber from the inlet is more than that from the outlet. In the pump process, the piezoelectric vibrator moves downward and the fluids are expelled from the pump chamber. Opposite to the suction process, the fluids discharged from the outlet are more than that from the inlet. Therefore, the micropump realises a one-way transportation. In a period, the net flow can be described as follows:

$$Q_{net} = \int_0^T q_o(t)\,dt, \tag{1}$$

where $q_o(t)$ is the transient flow rate and subscript o denotes the outlet.

2.2. Pump efficiency: The piezoelectric vibrator is composed of the piezoelectric ceramic (PZT), bonding layer and elastic plate, which is shown in Fig. 1.

In this Letter, the vibration model of the vibrator proposed by Bu *et al.* [12] was adopted. Compared with the PZT and elastic plate, the bonding layer is so thin that it can be ignored. Therefore, the model consists of two parts: central region (two-layer central circular with the radius a) and outer region (a ring with inner radius a and outer radius b). The deflections of the central and outer regions, respectively, denoted by $\omega_c(r)$ and $\omega_o(r)$ were deduced by Yang *et al.* [13]

$$\omega_c(r) = \omega_{max}\left(1 + \frac{b^2r^2 - a^2r^2}{2a^2b^2\ln(a/b)}\right) \quad (0 \le r \le a), \tag{2}$$

$$\omega_o(r) = \omega_{max}\left(\frac{b^2 + 2b^2\ln(r/b) - r^2}{2b^2\ln(a/b)}\right) \quad (a \le r \le b), \tag{3}$$

where ω_{max} is the maximum deflection of the central region and r is the radial distance from the central point of the vibrator.

The sinusoidal voltages were applied, such as the transient volume change of the pump chamber was obtained by integrating

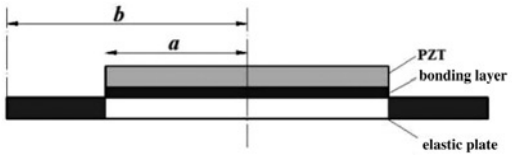

Fig. 1 *Structure of piezoelectric vibrator*

(2) and (3)

$$V_c(t) = \left(\int_0^a \omega_i(r) \times 2\pi r\,\mathrm{d}r + \int_a^b \omega_o(r) \times 2\pi r\,\mathrm{d}r\right)\sin(2\pi ft) = \omega_{\max}\frac{\pi(a^2-b^2)}{4\ln(a/b)}\sin(2\pi ft), \tag{4}$$

where f is the excitation frequency and t is the time.

Therefore, the volume changes of the pump chamber in a period can be expressed as

$$V_C = \omega_{\max}\frac{\pi(a^2-b^2)}{2\ln(a/b)}. \tag{5}$$

The pump efficiency is defined as the ratio of the net flow to the volume changes of the pump chamber, which is expressed as

$$\eta = \frac{Q_{\text{net}}}{V_c} = \frac{2\ln(a/b)\int_0^T q_o(t)\,\mathrm{d}t}{\omega_{\max}\pi(a^2-b^2)} = \frac{\sqrt{\lambda}-1}{\sqrt{\lambda}+1}, \tag{6}$$

where λ is the diffuser efficiency ($\lambda = \xi_n/\xi_d$), ξ_n and ξ_d are the pressure loss coefficients in converging and diverging flow, respectively [14]. Therefore, in order to improve the efficiency of the valveless piezoelectric micropump, it is important to increase the diffuser efficiency to obtain a higher flow rate. In this Letter, the concave tuning diffuser/nozzle element was applied in the valveless piezoelectric micropump, which could improve the diffuser efficiency tremendously and has been reported by Arvind Chandrasekaran *et al.* It is feasible for the micropump with a concave tuning diffuser/nozzle element to obtain higher pump efficiency, compared with the tradition valveless piezoelectric picropump with a straight-wall diffuser.

The characteristic Reynolds number Re_c is defined as

$$\mathrm{Re}_c = \frac{\mathrm{Re}_{i-\max} + \mathrm{Re}_{o-\max}}{2}, \tag{7}$$

where $\mathrm{Re}_{i-\max}$ and $\mathrm{Re}_{o-\max}$ are the maximum transient Reynolds numbers at the throat of the inlet and outlet, respectively.

The relationship between volume changes (V_c), the maximum transient velocities at the throat of the inlet channel ($u_{i-\max}$) and outlet channel ($u_{o-\max}$) is

$$\int_0^{T/2}\left(u_{i-\max} + u_{o-\max}\right)\sin(2\pi ft) \times A_c\,\mathrm{d}t = V_c. \tag{8}$$

Based on (7) and (8), Re_c can be expressed as

$$\mathrm{Re}_c = \frac{\pi^2(a^2-b^2)}{4\nu h\ln(a/b)} \times \omega_{\max} f. \tag{9}$$

where Re_c is proportional to the volume change rate, so Re_c can be seen as the dimensionless parameter of volume change rate. In order to analyse the influence of $\omega_{\max}$ and f independently, an assumption was proposed that Re_c is fixed. The relationships between $\omega_{\max} \times f$ and Re_c are given in Table 1.

3. Fabrication of micropump

3.1. Structural parameters: The schematic of a micropump with a conventional diffuser/nozzle element is shown in Fig. 2*a*. The chamber of the valveless piezoelectric micropump is connected to the inlet and outlet through the symmetrically positioned microdiffuser, the flow direction in the micropump results from the differential pressure drop across the diffuser/nozzle element [15]. The flow in the diffuser direction is taken as the positive direction and the flow in the nozzle direction and the flow in the nozzle direction is taken as the negative. The diffuser is connected between two channels of the cross-sectional area, the section of the least cross-sectional area of the diffuser is referred to as the throat. For the flow in the positive direction, the throat forms the inlet. Conversely, the flow in the negative direction exits through the throat. The width of the throat W_t and the depth of the channel H are both 200 μm; the radius of the throat is 0.1 mm; the radius of the inlet R_i and that of the outlet R_o are both 0.5 mm; the radius of PZT a is 4.5 mm; the radius of the elastic plate is 5 mm; the aspect ratio of the microchannel is 15; the width d_1 and length d_2 of the buffer chamber are 5.5 and 6 mm, respectively.

The expression of the channel width based on the concave tuning is given as follows:

$$W(x) = W_t + (W_o - W_t)x^{\beta_{cv}}, \tag{10}$$

Table 1 Characteristic Reynolds number under different $\omega_{\max} \times f$

$\omega_{\max} \times f$, μm s^{-1}	Re_c
180	100.11
540	300.34
900	500.57
1260	700.80
1800	1001.15

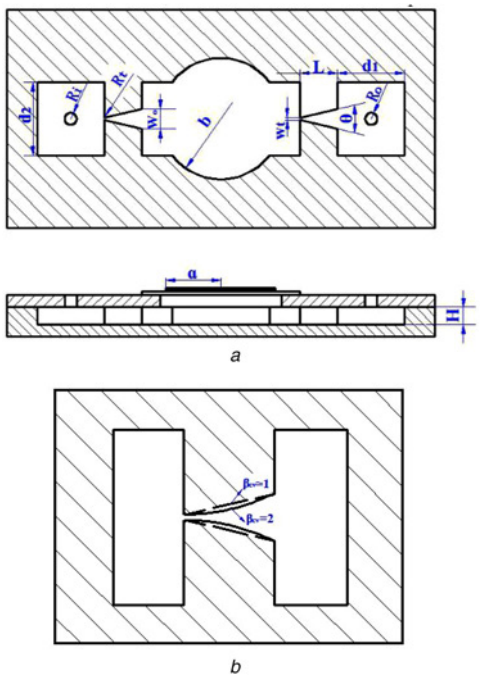

Fig. 2 *The geometric tuning of the micropump with conventional diffuser/nozzle element*
a Schematic of micropump with conventional diffuser/nozzle elements
b Concave tuning of straight channel

doi: 10.1049/mnl.2018.5712

where x is the non-dimensional length, β_{cv} is the tuning parameter ($\beta_{cv} = 1$ represents the straight sidewall). The channel structure with the concave tuning ($\beta_{cv} = 2$) is shown in Fig. 2*b*.

3.2. Fabrication: Compared with other materials, fabricating a polymer is easier, and its applications can reduce the time and cost of the manufacturing processes. Polydimethylsiloxane (PDMS) is one of the most actively developed polymers for microfluidics, not only the transparent substrate facilitates flow visualisation, but PDMS is also helpful for machining accuracy [16].

In this study, two kinds of micropumps were fabricated with PDMS by X-ray lithographie, Galvanoformung and Abformtechnik (LIGA). The manufacturing processes based on the LIGA method are shown in Fig. 3. To fabricate the two kinds of valveless piezoelectric micropumps, the thick photoresist layer needs to be rubberised on the metal coating substrate. A pair of X-rays with high energy is generated to expose and develop the thick photoresist through the mask, and the three-dimensional structure of photoresist is formed. By electroplating and removing the photoresist, a separate metal structure is obtained, which is used as a mould for PDMS mould pressing. Then the PDMS substrate is formed by the mould. Finally, the glazing cover will be bonded in the PDMS substrate. The diagram of a micropump with conventional diffuser/nozzle elements and concave tuning geometric are shown in Fig. 4.

4. Simulations and experimental setup

4.1. Numerical simulations: The CFD software CFX was employed for the simulations, and the schematic of the computational domain is shown in Fig. 5. The shear-stress transport κ–ω model was adopted in the simulation because of the accurate prediction of flows with strong adverse pressure gradients (APGs) and boundary layer separation [17]. The dynamic mesh method was applied to simulate the deflection of the piezoelectric vibrator, and the pressure boundary conditions were applied to the inlet and outlet. The working medium is water of 25°C, and the kinetic viscosity is 0.8937×10^{-6} m^2/s, the initial state is stationary. No-slip conditions were applied to the walls.

The analysis of mesh and time step sensitivity is carried out. The mesh at the throat is dense due to the high velocity. The grid-independent analysis when $\beta = 2$, $\theta = 30°$, $\mathrm{Re} = 100$ and $f = 100$ Hz has been carried out. The results indicate that the grid number of 1.2 million is sufficient to meet the requirements of the simulation. What is more, the relative error is only 0.45% when the time step is 1/(50f). Hence, the time step setting at 1/(100f) was enough in this Letter.

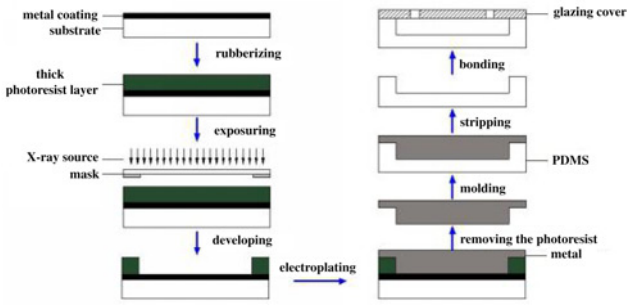

Fig. 3 *Manufacturing processes of the valveless piezoelectric micropump*

Fig. 4 *Photograph of micropumps*

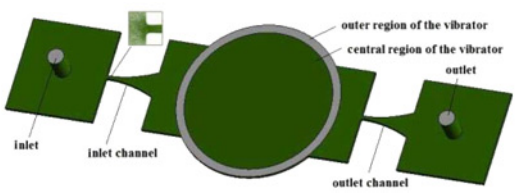

Fig. 5 *Computational domain of the micropump*

4.2. Experimental setup: The schematic of the experiments is shown in Fig. 6. The experimental apparatus includes a function generator (Tektronix, AFG3022B), a power amplifier (Fo Neng, HVP-300A), an oscilloscope (Tektronix, TBS1022), electronic scale (Jiming, JM-A.) etc.

The absolute alcohol was adopted to remove the air in the pump, and deionised water was used as the working fluid. A series of sinusoidal voltages with different frequencies and amplitudes were applied to drive the micropumps. The voltage and frequency were generated by the function generator that can provide the frequency of ranging from −2 to 1.000 MHz and the voltage of the maximum 20 Vpp, and then the voltage generated from the function generator was amplified by the power amplifier that could amplify the power outside ten times. The oscilloscope was employed to monitor the variation of the voltage, and the accurate voltage and frequency loaded in the micropump could be displayed in the oscilloscope. Since the voltage had been adjusted, the vibrator began the sinusoidal oscillation. After a period, the fluids in the tank had been sucked into the Petri dish. Finally, the mass flow in a period was measured by an electronic scale.

5. Results and discussions

5.1. Experimental results and discussions: Experiments were carried out to investigate the performance of the two kinds of micropumps with voltage ranging from 100 to 300 Vpp and excitation frequency ranged from 25 to 150 Hz. As $f = 100$ Hz, the variation of the net flow and pump efficiency with voltage has been shown in Fig. 7. The net flow increases with the increase of voltage, although the pump efficiency increases first and then decreases with the increase of voltage and the pump efficiency is the biggest when the voltage is 75 Vpp, which indicates that the increase of the volume changing rate is faster than the decrease of the pump efficiency.

Fig. 8 shows the variation of net flow and pump efficiency with excitation frequency as the voltage is 150 Vpp. The net flow and pump efficiency both reached the optimal value when $f = 300$ Hz,

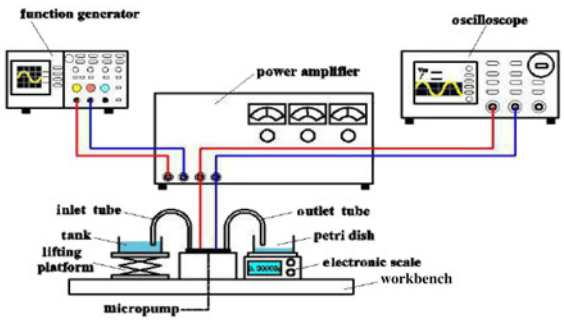

Fig. 6 *Schematic of the experiment*

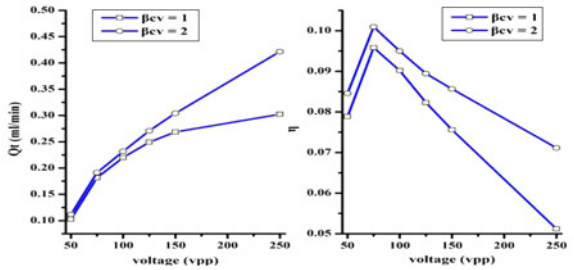

Fig. 7 *Variation of net flow and pump efficiency with voltage as f = 100 Hz*

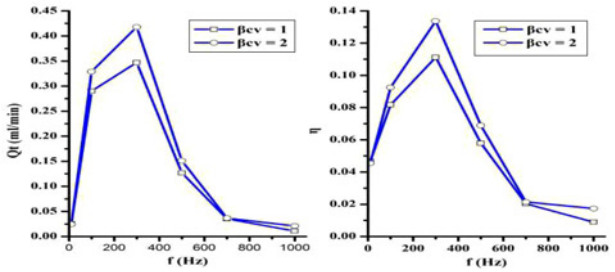

Fig. 8 *Variations of net flow and pump efficiency with frequency as V = 150 vpp*

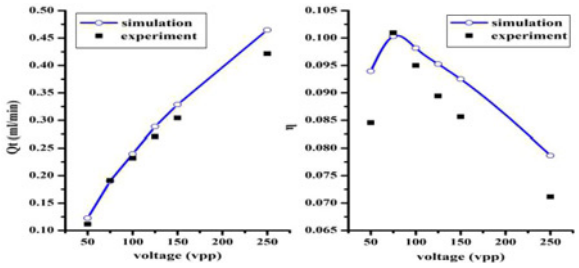

Fig. 9 *Comparison of the experiments and simulations as f = 100 Hz*

and the optimal pump efficiency of the micropump with a straight sidewall was improved by 20.3%.

5.2. Simulation results and discussions: Based on the results of membrane displacement experiments [10], the numerical simulations of the micropump with concave tuning were carried out as $f = 100$ Hz (see Fig. 9). The maximum error between experimental and simulation result is <11.1%, which verifies that the results in the simulation are reasonable.

5.2.1. Net flow: The net flow of the valveless piezoelectric micropumps with a straight sidewall ($\beta_{cv} = 1$) and concave tuning ($\beta_{cv} = 2$) is both presented in Fig. 10 as Re_c ranges from 100.11 to 1001.15 and f ranges from 10 to 1000 Hz. As the frequency is constant, the net flows of the two kinds of pumps both increase with the increase of Re_c. At different frequencies, the net flow of the micropump with concave tuning is higher than that of the micropump with a straight sidewall and the net flow was improved by 28.8% on average. Besides, the maximum net flow of micropumps with concave tuning can reach 1.18 ml/min.

5.2.2. Pump efficiency: When the excitation frequency ranged from 10 to 1000 Hz, the variation of pump efficiency of the two kinds of pumps with Re_c is shown in Fig. 11. At each frequency, the pump efficiency increases first and then decreases with the increase of Re_c. Moreover, the characteristic Reynolds number corresponding to the optimal pump efficiency increases with the increase of

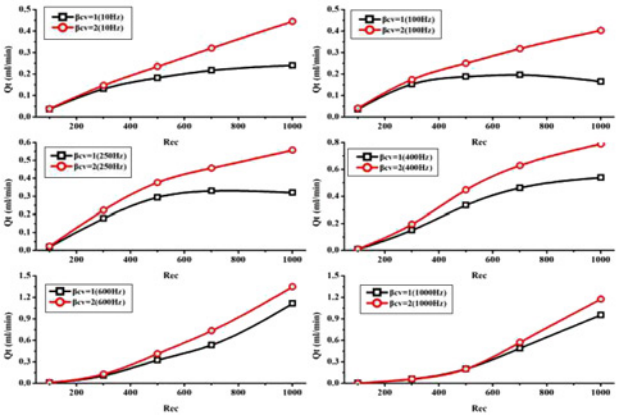

Fig. 10 *Variation of net flow with characteristic Reynolds number at different frequencies*

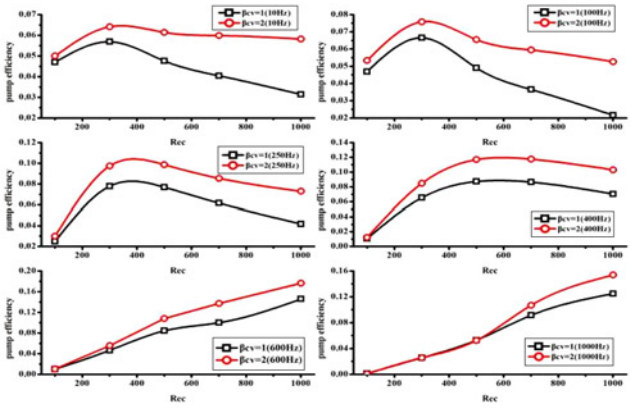

Fig. 11 *Variation of pump efficiency with characteristic Reynolds number at different frequencies*

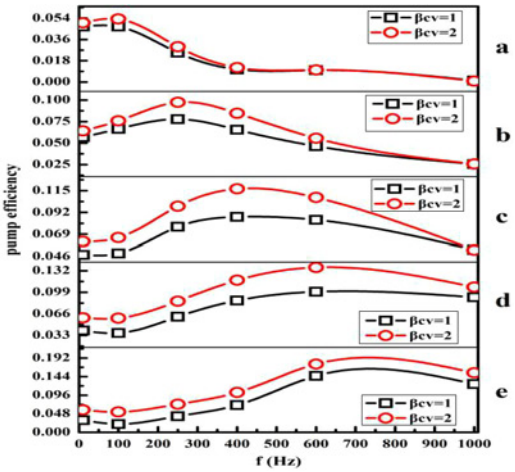

Fig. 12 *Variation of pump efficiency with excitation frequency under different Re_c*
a $Re_c = 100.11$
b $Re_c = 300.34$
c $Re_c = 500.57$
d $Re_c = 700.80$
e $Re_c = 1001.15$

frequency. Under different characteristic Reynolds numbers, the variation of the pump efficiency of two structures with excitation frequencies has been shown in Fig. 12. The pump efficiency of

doi: 10.1049/mnl.2018.5712

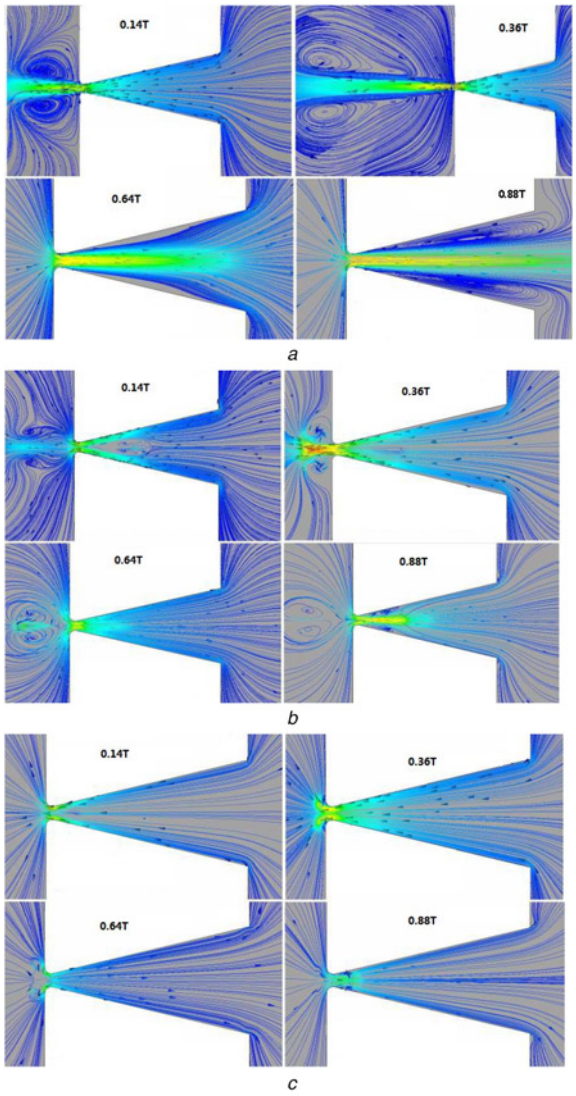

Fig. 13 *Streamline diagrams of the outlet channel with straight sidewall as* $Re_c = 300.34$
a $f = 10$ Hz
b $f = 250$ Hz
c $f = 1000$ Hz

the micropump with a straight sidewall was improved apparently by concave tuning. As the volume change rate of the pump chamber is constant, the variation of excitation frequency results in the variation of the optimal pump efficiency. The corresponding frequency is defined as the optimal excitation frequency, which increases with the increase of Re_c. When Re_c changed from 100.11 to 1001.15, the optimal excitation frequencies are 100, 250, 400, 600, and 700 Hz, respectively.

5.2.3. Internal flow characteristics: The pump efficiency of the two structures has the same changing trend under the same characteristic Reynolds numbers. The streamline diagrams of the outlet channel with straight sidewall is presented in Fig. 13 as $Re_c = 300.34$. In the suction process ($t = 0.14$ and 0.36 T), a pair of vortexes resulting from the shear flow was formed in the buffer chamber as $f = 10$ Hz.

When f increases to 250 Hz, two pairs of vortexes were, respectively, shown in the buffer chamber and outlet channel. As time goes on, the vortexes in the buffer chamber get closer to the throat. As $f = 1000$ Hz, the vortexes in the outlet channel disappeared soon. The intensity of the hindering function of the vortexes depends on the position and size of the vortexes, the shorter the distance

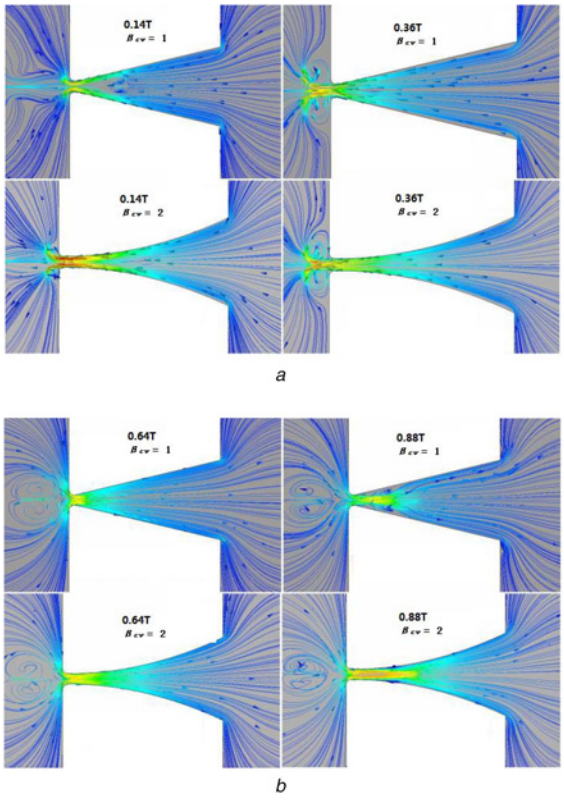

Fig. 14 *Streamline diagrams of the outlet channel as* $Re_c = 700.8031184$ *and* $f = 600$ *Hz*
a Suction process
b Pump process

to the throat and the larger the vortexes, the greater the flow resistance. Therefore, in the suction process, the flow resistance is the biggest when $f = 250$ Hz. In the pumping process ($t = 0.64$ and 0.88 T), as $f = 10$ Hz, the boundary layer separation is well developed in the channel. As $f = 250$ and 1000 Hz, the vortexes in the buffer chamber gradually disappeared and the effect region was always small, so the hindering function of vortexes is smaller than that of $f = 10$ Hz. As $f = 250$ and 1000 Hz, the vortexes in the buffer chamber gradually disappeared and the effect region was always small, so the hindering function of vortexes is smaller than that of $f = 10$ Hz when $f = 10$ Hz. According to (6), it was concluded that the pump efficiency increases as $10 \leq f \leq 250$ Hz and decreases as $250 \leq f \leq 1100$ Hz. The above analysis is a good qualitative explanation of the variation in Fig. 12*b*.

Compared with the straight sidewall, the micropump with a concave tuning diffuser/nozzle element performs better. The streamline diagrams of the two kinds of micropumps are presented in Fig. 14 as $Re_c = 700.80$ and $f = 600$ Hz. At high Reynolds number (referring to Fig. 14), in the suction process, the flow difference is not very obvious, two pairs of vortexes were formed in two micropumps. The pair near the throat became bigger and bigger as time goes on, and the other pair inside the channels disappeared after some time. However, in the pumping process, due to the boundary layer separation, the vortexes were formed inside the straight channel, which did not happen in the micropump with a concave tuning structure. Therefore, the diverging flow resistance in a straight channel was much larger than that in the concave tuning channel, and the pump efficiency is significantly improved by concave tuning as shown in Fig. 12*d*.

The distribution of the pressure in the outlet channel of the two kinds of micropumps is presented in Fig. 15. In the suction process, the pressure drop of the channel with concave tuning is larger than that of the channel with a straight sidewall. In the

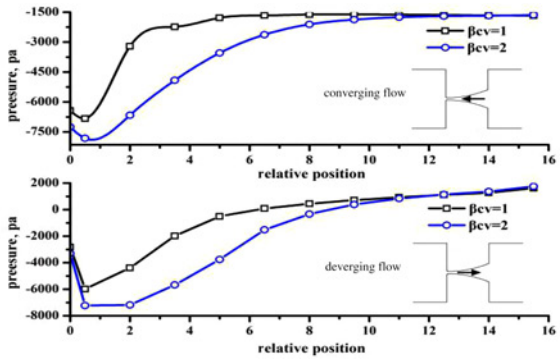

Fig. 15 *Distribution of the pressure along the outlet channel in the suction and pump process as $Re_c = 700.80$ and $f = 600$ Hz*

pumping process, the APG was formed in the two kinds of micropumps, but the APG was delayed by concave tuning, which was also larger than that in the straight channel. Therefore, the boundary layer separation in the concave tuning channel is limited in Fig. 14*b*.

6. Conclusions: In this study, the performances of valveless piezoelectric micropumps with a straight sidewall ($\beta_{cv} = 1$) and concave tuning structure ($\beta_{cv} = 2$) have been investigated by experimental and numerical simulation.

The experiment was carried out under conditions of voltage (50–250 vpp) and excitation frequency (10–1000 Hz). As $f = 100$ Hz, the net flow of two kinds of micropumps increases with the increase of voltage. While the pump efficiency increases first and then decreases with the increase of voltage, the optimal voltage is 75 Vpp. The net flow and pump efficiency of the valveless piezoelectric micropump with a straight sidewall can be improved by 28.8 and 20.3%, respectively, through concave tuning. As the voltage is 150 Vpp, the increase of excitation frequency results in the optimal net flow and pump efficiency. The corresponding frequency is defined as the optimal frequency, of which the value is 300 Hz.

The numerical simulation was carried out under the conditions of Re_c (100–1000) and excitation frequency (10–1000 Hz). Compared with experimental results, the maximum error of numerical simulation is <11.1%, herein, the simulation method is reliable. At the same frequency, the increase of Re_c resulted in an increase in the optimal pump efficiency and the corresponding characteristic Reynolds number increased with the increase of frequency. When the volume change rate is constant, the variation of frequency also results in variation of the optimal pump efficiency, and the corresponding frequency increases with the increase of Re_c. The position and size of vortexes are of great significance to the performances of the micropump. Compared with the micropump with a straight sidewall, that with concave tuning structure can better withstand the APG and delay the boundary layer separation in the channel, therefore, the performances of the micropump with a straight sidewall were well improved by concave tuning.

7. Acknowledgments: This work was supported by the project of the National Natural Science Foundation of China [grant no. 51276082]. Departments of Education and Finance, Jiangsu Province of People's Republic of China (A Project Funded by the Priority Academic Program Development of Jiangsu Higher Education institutions, PAPD) [grant no. SUZHENGBANFA (2014) no. 37].

8 References

[1] Ballato A.: 'Piezoelectricity: old effect, new thrusts', *Proc. IEEE Trans. Ultrason. Ferroelectr. Freq. Control*, 1995, **42**, (5), pp. 916–926

[2] Iverson B.D., Garimella S.V.: 'Recent advances in microscale pumping technologies: a review and evaluation', *Microfluid. Nanofluid.*, 2008, **2**, (5), pp. 145–174

[3] Woias P.: 'Micropumps-past, progress and future prospects', *Sens. Actuators B*, 2005, **105**, pp. 28–38

[4] Laser D.J., Santiago J.G.: 'A review of micropumps', *J. Micromech. Microeng.*, 2004, **14**, (6), pp. 35–64

[5] Jiang X.N., Zhou Z.Y., Huang X.Y., *ET AL.*: 'Micronozzle/diffuser flow and its application in micro valveless pumps', *Sens. Actuators A, Phys.*, 1998, **70**, (1), pp. 81–87

[6] Chandrasekaran A., Packirisamy M.: 'Geometrical tuning of microdiffuser/nozzle for valveless micropumps', *J. Micromech. Microeng.*, 2011, **21**, p. 045035

[7] Chandrasekaran A., Packirisamy M.: 'Improved efficiency of microdiffuser through geometry tuning for valveless micropumps', *J. Fluids Eng.*, 2016, **138**, p. 031101-1

[8] Olsson A., Stemme G., Stemme E.: 'Numerical and experimental studies of flat-walled diffuser elements for valve-less micropumps', *Sens. Actuators A, Phys.*, 2000, **84**, pp. 165–175

[9] Sun X., Jiang D., Yang Z.: 'Structural design and performance test of serial-three-chamber piezoelectric pump', *Paiguan Jixie Gongcheng Xuebao/J. Drainage Irrigation Mach. Eng.*, 2014, **32**, (5), pp. 388–392

[10] He X.H., Zhu J.W., Zhang X.T., *ET AL.*: 'The analysis of internal transient flow and the performance of valveless piezoelectric micropumps with planar diffuser/nozzles elements', *Microsyst. Technol.*, 2015, **23**, (1), pp. 1–15

[11] He X.H., Yang S., Yuan S.Q., *ET AL.*: 'Design of a novel bidirectional valveless piezoelectric micropump with three chambers using Coanda effect based on numerical simulation'. Proc. ASME 2014 4th Joint US-European Fluids Engineering Division Summer Meeting, 2014, p. V01BT10A021

[12] Bu M., Tracy M., Graham E.: 'Design and theoretical evaluation of a novel microfluidic device to be used for PCR', *J. Micromech. Microeng.*, 2003, **13**, pp. S125–S130

[13] Yang S., Yuan S.Q., Cai S.C., *ET AL.*: 'A valveless piezoelectric micropump based on Coanda effect', *Trans. Chin. Soc. Agric. Mach.*, 2014, **45**, pp. 343–348

[14] Wang Y.C., Hsu J.C., Kuo P.C., *ET AL.*: 'Loss characteristics and flow rectification property of diffuser valves for micropump applications', *Int. J. Heat Mass Transf.*, 2009, **52**, (1), pp. 328–336

[15] Stemme E., Stemme G.: 'A valveless diffuser/nozzle-based fluid pump', *Sens. Actuators A*, 1993, **39**, pp. 159–167

[16] Jeong O.C., Park S.W., Yang S.S., *ET AL.*: 'Fabrication of a peristaltic PDMS micropump', *Sens. Actuators A, Phys.*, 2005, **123**, pp. 453–458

[17] Menter F.R., Kuntz M., Langtry R.: 'Ten years of industrial experience with the SST turbulence model'. Proc. 4th Int. Symp. on Turbulence, Heat and Mass Transfer, Antalya, Turkey, 12–17 October 2003, pp. 625–663

doi: 10.1049/mnl.2018.5712